Localization of chaos in the discrete nonlinear Schrödinger equation

N. Finlayson and K. J. Blow
BT Laboratories, Martlesham Heath, Ipswich IP5 7RE, United Kingdom

L. J. Bernstein
Mathematics Department, Idaho State University, Pocatello, Idaho 83209

K. W. DeLong
Sandia National Laboratories, Livermore, California 94551-0969
(Received 16 February 1993)

We partition the perturbation phase space in the three-element discrete nonlinear Schrödinger equation into symmetric and antisymmetric subspaces. We then show that chaotic motion in the neighborhood of symmetric trajectories is confined to the antisymmetric space. Chaos occurs in the system at arbitrarily low levels of nonlinearity, in agreement with previous calculations. We call this phenomenon "microchaos."

PACS number(s): 42.50.Lc, 05.45.+b, 03.65.Ge

I. INTRODUCTION

The phenomenon we choose to call "microchaos" is a condition in which chaos in a Hamiltonian nonlinear dynamical system persists even when the nonlinearity is reduced to an arbitrarily low but nonzero level. This situation is in marked contrast with systems described by the Kolmogorov-Arnold-Moser (KAM) theorem where it is always possible to reduce the strength of the nonlinear perturbation such that regular motion is recovered [1]. Microchaotic systems are distinguishable from KAM systems in that the unperturbed microchaotic system is both linear and intrinsically degenerate, i.e., the unperturbed oscillator frequencies satisfy simple low-order resonance relations [1]. Consequently, the linear system is in an *already critical* state such that the addition of arbitrarily small nonlinearity can lead immediately to chaotic motion. Microchaos was first described by Ford and Lunsford in 1970 [2] and was subsequently also discussed by Contopolous [3]. Further references to microchaos in the literature are relatively rare, although it is likely that the phenomenon is quite ubiquitous. Here we discuss a particular example of microchaos which arises in the discrete nonlinear Schrödinger equation (DNLSE).

The occurrence of microchaos in the DNLSE was originally observed in numerical experiments [4]. The DNLSE [5] can be used to model optical field propagation in weakly coupled waveguide lattices and the three-element open lattice has been studied in some detail [4,6–10]. An analysis of microchaos in the limit ($Q \rightarrow 0$) in the three-element lattice has been given in Ref. [10]. We shall show here that an essential feature of chaotic motion (including microchaos) in the three-element DNLSE *in the vicinity of symmetric excitations* is localization in antisymmetric regions of the perturbation phase space. Localization occurs because (i) symmetric excitations are fully integrable [4,10] and (ii) the motion of symmetric and antisymmetric perturbations are independent to first order. We shall explore the consequences of this observation further in this paper thereby taking the opportunity to clarify the underlying physics outlined in Ref. [10].

In Sec. II we briefly review the Ford-Lunsford procedure for analyzing resonant Hamiltonians, making specific reference to the Hamiltonian governing our three-element DNLSE. We then discuss a technique used for quantifying the degree of chaos in the DNLSE, namely, the calculation of Lyapunov exponents for the system. The main result of the paper is that chaotic motion associated with small perturbations to symmetrical trajectories of the three-element lattice is confined to the antisymmetric subspace, to first order in the perturbation. We present a compact algorithm for estimating accurately the two nonzero Lyapunov exponents which involves only perturbative motion in the antisymmetric subspace. This algorithm shows excellent agreement with the more complex procedure previously adopted [4].

II. THE RESONANT HAMILTONIAN

We briefly outline the fundamental characteristics of microchaos, using the open three-element DNLSE lattice as a specific example and closely following the discussion of Ford and Lunsford [2]. A Hamiltonian for the three-element open DNLSE lattice may be written in terms of the local field variables $a_k = |a_k| \exp(i\phi_k)$ at each lattice site k as follows:

$$H = \kappa[|a_1||a_2|\cos(\phi_1-\phi_2)+|a_2||a_3|\cos(\phi_2-\phi_3)] + \frac{Q(|a_1|^4+|a_2|^4+|a_3|^4)}{4}, \quad (1)$$

where κ is a linear constant coupling the field a_k to its nearest neighbors and Q is a parameter characterizing the strength of the nonlinearity. A change of variables to the linear eigenmodes for the lattice results in a Hamiltonian of the form

 ©1993 The American Physical Society

$$H=\beta_1 J_1+\beta_2 J_2+\beta_3 J_3+\frac{Q}{4}[V_{\text{res}}(\mathbf{J},\boldsymbol{\theta})+V_{\text{nonres}}] , \tag{2}$$

where $J_m=|b_m|^2/2$ and $b_m=|b_m|\exp(i\theta_m)$ is the complex field amplitude of the mth linear eigenmode. The linear eigenmode frequencies given by ($\beta_1=\sqrt{2}\kappa$, $\beta_2=0$, $\beta_3=-\sqrt{2}\kappa$) satisfy the linear resonance relation

$$\sum_{i=1}^{3} n_i\beta_i=0 , \tag{3}$$

where the n_i are small integers. V_{res} is a nonlinear function of the eigenmode fields given by

$$V_{\text{res}}=\left[\frac{3J_1^2}{2}+4J_1J_2+2J_2^2+6J_1J_3+4J_2J_3+\frac{3J_3^2}{2}-4J_1^{1/2}J_2J_3^{1/2}\cos(\theta_1-2\theta_2+\theta_3)\right] . \tag{4}$$

Each individual term in V_{res} has zero Poisson bracket with the linear part of the Hamiltonian [1], implying that these nonlinear terms are *resonant* with the linear part of the Hamiltonian, i.e., the linear and nonlinear terms are phase matched. The last term on the right-hand side (rhs) of Eq. (4) is the only term which gives rise to coupling among the internal degrees of freedom of the system. The occurrence of zero Poisson bracket for this term is *conditional* on the linear resonance given by Eq. (3). Drastic modification of the system orbits can occur owing to the coexistence of linear and nonlinear resonance in this Hamiltonian.

V_{nonres} contains the remaining nonresonant nonlinear terms in the Hamiltonian. At low Q, the only effect of the nonresonant terms is to slightly distort the orbits of the system [2]. In the limit $Q\to 0$, V_{nonres} can be ignored. The linear terms can be removed from the Hamiltonian using the mixed variable generating function

$$F=\sum_{i=1}^{m}(\bar{J}_i)(\theta_i-\beta_i z) . \tag{5}$$

We are left with a Hamiltonian of the form

$$H=\frac{Q}{4}V_{\text{res}} . \tag{6}$$

The prefactor $Q/4$ appears purely as a multiplicative constant in the Hamiltonian and it therefore primarily determines the length scale of the motion. The remarkable consequence is that any chaotic behavior manifested in Hamiltonian (6) will persist to arbitrarily low though nonzero values of Q. As first pointed out by Ford and Lunsford [2] this type of behavior can be expected for any system governed by a Hamiltonian of the form shown in Eq. (2). The length scaling properties of Hamiltonian (6) imply that the largest positive Lyapunov exponent characterizing chaos will diminish in proportion to Q, hence the term *microchaos*.

III. MOTION IN THE THREE-ELEMENT LATTICE

Bearing the above discussion in mind, we begin our analysis of motion in the three-element open DNLSE lattice. We restrict our attention to (a) spatial field variations and (b) small perturbations about symmetric lattice excitations. The three-element DNLSE derived directly from Eq. (1) has the form

$$\frac{da_1}{dz}=i\kappa a_2+iQ|a_1|^2a_1 , \tag{7a}$$

$$\frac{da_2}{dz}=i\kappa(a_1+a_3)+iQ|a_2|^2a_2 , \tag{7b}$$

$$\frac{da_3}{dz}=i\kappa a_2+iQ|a_3|^2a_3 . \tag{7c}$$

The symmetric excitations of the three-element lattice given by $a_1=a_3$ are fully integrable and solutions may be written in the form of Jacobi elliptic functions [10].

To detect the occurrence of chaos in six-dimensional phase space it is usually necessary to consider the evolution of a six-dimensional sphere of small perturbations into an ellipsoid under the influence of a reference or "fiducial" trajectory $\mathbf{a}(z)$ [4,11]. In general, a linearized perturbation vector $\boldsymbol{\epsilon}(z)$ will experience a change in its Euclidean norm $r(z)$ as a result of this evolution. Locally, most perturbation vectors will be reoriented in the direction of largest growth of the ellipsoid [11]. To calculate the global behavior of such a vector, we initialize it as a unit vector, propagate it a distance Δz under the influence of the fiducial trajectory, and calculate its resultant norm. To obtain accurate results, the propagation distance Δz is chosen to be much smaller than the characteristic beat length set by the linear eigenmodes. We define a local exponent $\rho(z)$ where

$$\rho(z)=\frac{1}{\Delta z}\log_2 r(z) . \tag{8}$$

To avoid problems with the occurrence of exponential growth we then normalize the resultant vector magnitude to unity without changing its orientation, and repeat the procedure. After an initial transient, the global record of the steady-state behavior of the local exponents is obtained as $z\to\infty$. The global behavior can be periodic in which case it is sufficient to evolve the perturbation over one period after the decay of the transient. Note that periodic evolution refers to the *renormalized* vector, and that chaotic motion is possible in such a case: chaos corresponding to long-range exponential growth occurs where the local exponents are positive on average. The resulting average value defines the most positive Lyapunov exponent for the system.

IV. LOCALIZATION OF CHAOTIC MOTION

Excitations of the three-element DNLSE containing projections into the antisymmetric subspace have been shown to lead to chaos and microchaos [4,7]. The antisymmetric subspace constitutes a two-dimensional cross section of the full six-dimensional phase space. To first order in the perturbation strength the motion of small perturbations in the vicinity of symmetric fiducial trajectories is separable into independent components projecting onto symmetric and antisymmetric subspaces. To see

this, we first write the linearized equations for symmetric fiducial trajectories ($a_1=a_3$):

$$\frac{d\epsilon_1}{dz}=i\kappa\epsilon_2+iQ(2|a_1|^2\epsilon_1+a_1^2\epsilon_1^*)\ , \tag{9a}$$

$$\frac{d\epsilon_2}{dz}=i\kappa(\epsilon_1+\epsilon_3)+iQ(2|a_2|^2\epsilon_2+a_2^2\epsilon_2^*)\ , \tag{9b}$$

$$\frac{d\epsilon_3}{dz}=i\kappa\epsilon_2+iQ(2|a_1|^2\epsilon_3+a_1^2\epsilon_3^*)\ . \tag{9c}$$

It is convenient to write the perturbation vector ϵ as an exact linear superposition of symmetric components $\epsilon_e=[\epsilon_2,\epsilon_s]$ and an antisymmetric component $\epsilon_o=[\epsilon_{as}]$ where $\epsilon_s=\epsilon_1+\epsilon_3$, $\epsilon_{as}=\epsilon_1-\epsilon_3$. We then obtain linearized equations of the form

$$\frac{d\epsilon_2}{dz}=i\kappa\epsilon_s+iQ(2|a_2|^2\epsilon_2+a_2^2\epsilon_2^*)\ , \tag{10a}$$

$$\frac{d\epsilon_s}{dz}=2i\kappa\epsilon_2+iQ(2|a_1|^2\epsilon_s+a_1^2\epsilon_s^*)\ , \tag{10b}$$

$$\frac{d\epsilon_{as}}{dz}=iQ(2|a_1|^2\epsilon_{as}+a_1^2\epsilon_{as}^*)\ . \tag{10c}$$

Treating the fiducial fields a_1 and a_2 as z-dependent coefficients, it is clear that the symmetric and antisymmetric subspaces are uncoupled, i.e., the symmetric and antisymmetric vector components are linearly independent. Note that the retention of higher-order perturbation terms or the breaking of symmetry in the fiducial field (such that $a_1\neq a_3$) leads to the loss of independence.

Linear independence in the first-order limit implies that we may propagate the symmetric and antisymmetric components separately. By virtue of (i) the integrable nature of symmetric fiducial trajectories [10] and (ii) the linear independence of the linearized equations, Eqs. (10a) and (10b) are *guaranteed* to exhibit regular behavior since a symmetric perturbation to a symmetric fiducial trajectory yields a symmetric resultant.

Consequently, the central result of this paper may be stated as follows: In the vicinity of symmetric fiducial trajectories of the three-element open DNLSE lattice, exponential contraction and expansion of the linearized flow can take place *on average* only in the antisymmetric subspace. *Local* expansion and contraction in the symmetric subspace is not prohibited; however, such changes must average to zero eventually. For the six-dimensional Hamiltonian system under consideration, therefore, four Lyapunov exponents are guaranteed to be zero owing to the integrability of the four-dimensional symmetric trajectories. Any remaining nonzero exponents are associated with motion in the antisymmetric plane. Since the system is Hamiltonian the magnitudes of the positive and negative Lyapunov exponents are guaranteed to be equal.

It is clear therefore that in the presence of certain symmetries chaos in the three-element DNLSE is of an unusual character: (a) it persists to arbitrarily low levels of nonlinearity and can consequently be classified as microchaos and (b) it is confined to a readily distinguishable cross section of the phase space, in contrast with the extreme complexity of the chaotic web generally observed.

V. MOTION OF A RANDOMLY CHOSEN VECTOR

We now consider the motion of an arbitrary perturbation vector in the six-dimensional phase space in the presence of on-average exponential growth and contraction. We have established that such growth and contraction is confined to the antisymmetric plane. Exponential growth of the antisymmetric components in comparison with zero on-average growth of the symmetric components means that the relative magnitudes of antisymmetric to symmetric components grows rapidly with propagation distance. A randomly selected vector will then evolve such that it eventually sits completely in the antisymmetric plane. This process is illustrated in Fig. 1, which was calculated using the numerical technique described in Ref. [4]. The standard practice of frequent renormalization of the vector norm to unity was used to keep the vector in bounds. The fiducial trajectory was set by launching all the power initially into the center element of the lattice. The evolution of the small perturbations is such that the vector eventually sits in the antisymmetric space defined by $\epsilon_1=-\epsilon_3$, $\epsilon_s=\epsilon_2=0$. This behavior holds true for any perturbation vector with a component initially pointed in the direction of largest growth [11], subject to the condition that chaotic motion actually occurs. The evolution of the *renormalized* vector is periodic thereafter, with the period of the fiducial trajec-

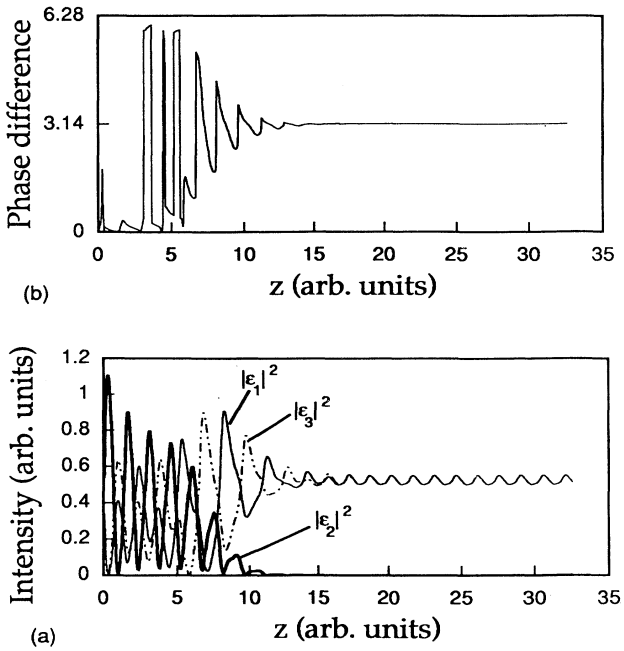

FIG. 1. Evolution of a first-order perturbation vector in the vicinity of the trajectory where the central lattice element is initially excited. $\kappa=1$, $I=1$, $Q=2.0$. (a) Intensities of each perturbation component. Thin solid line, $|\epsilon_1|^2$. Thick solid line, $|\epsilon_2|^2$. Dotted line, $|\epsilon_3|^2$. (b) Phase difference between ϵ_1 and ϵ_3. After an initial transient the perturbation intensities in the outer lattice elements become equal, the central element perturbation intensity decays to zero, and the phase difference becomes equal to π.

tory: a nonzero average for the change in the norm then yields a positive Lyapunov exponent, denoting the occurrence of chaos.

It is evident that the transient period during which the perturbation vector gets pulled onto the antisymmetric subspace is essentially wasteful in terms of characterizing the degree of chaos and the perturbation vector may as well be constrained to sit in the antisymmetric plane from the outset. It is then necessary only to consider the evolution of the complex vector $\epsilon_{as}=|\epsilon_{as}|\exp(i\alpha)$ using Eq. (10c). Notice that there is a direction in the antisymmetric plane on which the projection of the direction of largest growth has a theoretically zero component. With finite precision arithmetic this direction is essentially inaccessible. However, a perturbation vector lying in the neighborhood of this direction rotates relatively slowly in the direction of largest growth and a corresponding second transient becomes evident in the motion. Eventually the rotation of the vector in the antisymmetric plane becomes fully driven by the fiducial trajectory [10]. The largest Lyapunov exponent is calculated from the subsequent motion.

Siting the perturbation vector in the antisymmetric subspace has two advantages over the procedure used previously [4]. Firstly, the dimensionality of the linearized motion is reduced from six to two. Secondly, the local motion of the perturbation vectors reduces to an eigenvalue problem which can be solved exactly. In contrast, the procedure previously used required numerical integration (fourth-order Runge-Kutta) of a six-dimensional perturbation equation [4].

VI. DETAILS OF THE MODEL

Without loss of generality the total intensity of the fiducial trajectory $I=2|a_1|^2+|a_2|^2$ and the coupling constant κ can be set to unity. The dynamical behavior is then characterized completely by the nonlinear parameter Q. The calculation of the motion of small perturbations around the fiducial trajectory may be achieved using the linearized equations of motion for the antisymmetric components of the perturbation Eq. (10c). These may be written in terms of the complex perturbation field $\epsilon_{as}=\xi+i\zeta$ as

$$\frac{d}{dz}\begin{bmatrix}\xi\\ \zeta\end{bmatrix}=\mathbf{J}\begin{bmatrix}\xi\\ \zeta\end{bmatrix}, \tag{11}$$

where

$$\mathbf{J}=\begin{bmatrix}B & A\\ C & -B\end{bmatrix} \tag{12}$$

and A, B, and C are real z-dependent functions of the complex field $a_1=|a_1|\exp(i\phi_1)$ given by

$$\begin{aligned}A&=-Q|a_1|^2(1+2\sin^2\phi_1),\\ B&=-Q2|a_1|^2\sin(\phi_1)\cos\phi_1,\\ C&=Q|a_1|^2(1+2\cos^2\phi_1).\end{aligned} \tag{13}$$

Equation (11) can be written in the form of a Mathieu-Hill equation and treated using the techniques of Floquet theory [12]. Rather than perform such an analysis here, we use a mapping to calculate local exponents in the antisymmetric subspace in terms of the eigenvalues and eigenvectors of the matrix $\mathbf{J}$. The eigenvectors associated with motion in this subspace are the column vectors of the following matrix:

$$\mathbf{P}=\begin{bmatrix}A & A\\ -B+\lambda & -B+\lambda^*\end{bmatrix}, \tag{14}$$

where the asterisk denotes complex conjugation. The eigenvalues are purely imaginary and are given by

$$\begin{aligned}\lambda&=iQ\sqrt{3}|a_1|^2,\\ \lambda^*&=-iQ\sqrt{3}|a_1|^2.\end{aligned} \tag{15}$$

The *local* motion of perturbations in the antisymmetric subspace can be described exactly in terms of phase rotations in the eigenvector basis:

$$\begin{bmatrix}\xi(\Delta z)\\ \zeta(\Delta z)\end{bmatrix}=\mathbf{PLP}^{-1}\begin{bmatrix}\xi(0)\\ \zeta(0)\end{bmatrix}, \tag{16}$$

where $\xi(0)$ and $\zeta(0)$ are initial conditions and the matrix $\mathbf{L}$ is given by

$$\mathbf{L}=\begin{bmatrix}e^{\lambda\Delta z} & 0\\ 0 & e^{\lambda^*\Delta z}\end{bmatrix}. \tag{17}$$

Note that the transformation $\mathbf{PLP}^{-1}$ is not orthogonal so that norm conservation does not occur even though the eigenvalues are purely imaginary. If we normalize the initial condition such that $\xi(0)^2+\zeta(0)^2=1$ and allow the phase $\tan^{-1}[\zeta(0)/\xi(0)]$ to vary from 0 to 2π, Eq. (16) describes the mapping of an initially circular neighborhood of the fiducial trajectory onto an ellipse. The ellipse has equation

$$\frac{x^2}{g^2}+g^2y^2=1 \tag{18}$$

in a basis defined by the primary ellipse axes. The major axis length g is found from Eq. (16) to be

$$g=1+\frac{1}{\sqrt{3}}|\lambda|\Delta z, \tag{19}$$

where we have invoked the small angle approximation $\sin(|\lambda|\Delta z)\approx|\lambda|\Delta z$. The primary axes lengths $(g,1/g)$ define the maximal bounding values that local contraction and expansion exponents can take and we henceforth refer to the ellipse described by Eq. (18) as the "bounding ellipse." The bounding values of the local exponent are given by

$$\begin{aligned}\rho_{jb}&=\pm\frac{1}{\Delta z}\frac{\ln g}{\ln 2}\\ &=\pm\frac{Q|a_1|^2}{\ln 2}.\end{aligned} \tag{20}$$

In general, the local direction of largest growth in the antisymmetric space does *not* coincide with the orientation of the renormalized perturbation vector. Indeed, the per-

turbation vector can rotate *away from* the major axis as they both evolve. This is illustrated in the schematic of Fig. 2, which successively depicts a circle→ellipse →renormalization→circle→ellipse evolution. In Fig. 2(a) the perturbation vector is oriented at an angle δ with respect to the axes along which maximal growth and contraction occur. In Fig. 2(b) the mapping defined by Eq. (16) transforms the circle to an ellipse. Rotation of the perturbation vector towards the major axis of the ellipse *has* to occur during this step, i.e., the vector tends to align itself with the major axis. In Fig. 2(c) renormalization has taken the perturbation vector back onto the unit circle while preserving the orientation angle δ'. A further application of the mapping of Eq. (16) generates a new ellipse and the perturbation vector is again rotated towards the major axis to the new angle δ''. However, in going from Fig. 2(c) to Fig. 2(d) the ellipse itself has rotated under the action of the mapping. The next effect is that the angle between the perturbation vector and the ellipse major axis has *increased* from ϕ to ϕ'. This can result in the vector actually experiencing net contraction giving rise to a negative local exponent.

Over certain propagation distances, therefore, the local rates of ellipse and vector reorientation can be mismatched. Whether the angle between ellipse major axis and the perturbation vector increases or decreases depends upon the fiducial field. In the steady state the major axis and the perturbation vector are driven by the fiducial field such that the perturbation vector precesses around the ellipse major axis. The details of the angular motion executed by the perturbation vector then determine whether or not the system is chaotic.

In general, therefore, it is not sufficient to track only the variation of the ellipse axes. The local exponent associated with the evolution of the perturbation vector around the ellipse must be monitored. The local exponents may be calculated using successive applications of the following mapping, derived from Eq. (16):

$$\xi_{j+1}=\frac{1}{r_j}[(1+B_j\Delta z)\xi_j+A_j\Delta z\zeta_j]\ , \tag{21}$$

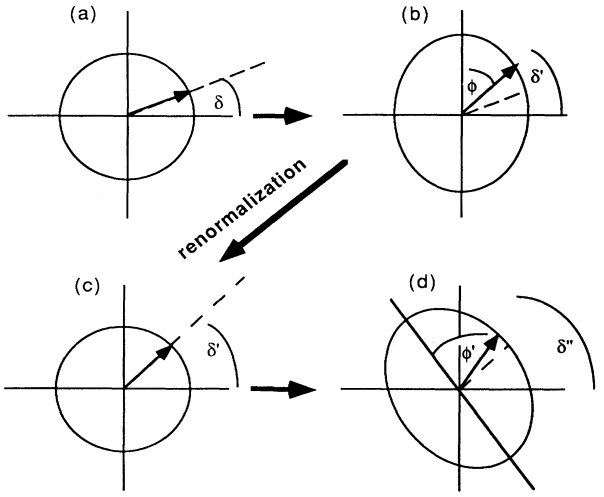

FIG. 2. Schematic of a circle→ellipse→renormalization →circle→ellipse cycle.

$$\zeta_{j+1}=\frac{1}{r_j}\left[-\frac{(B_j^2+|\lambda|^2)\Delta z}{A_j}\xi_j+(1-B_j\Delta z)\zeta_j\right]\ , \tag{22}$$

$$r_j^2=1+2B_j(\xi_j^2-\zeta_j^2)\Delta z+2\frac{\xi_j\zeta_j\Delta z}{A_j}(A_j^2-B_j^2-|\lambda|^2)\ , \tag{23}$$

where the coefficients A_j, B_j, and $|\lambda_j|$ are the quantities A, B, and $|\lambda|$ evaluated from analytical expressions for the fiducial trajectory at each propagation point $z=j\Delta z$. Equations (21)–(23) are derived in the limit $\Delta z\ll 1$ which is necessary to ensure that only local stretching is measured [11]. The local exponent is in this limit is given by

$$\rho_j=\frac{1}{\Delta z}\log_2 r_j$$
$$=\frac{1}{\ln 2}\left[B_j(\xi_j^2-\zeta_j^2)+\frac{\xi_j\zeta_j}{A_j}(A_j^2-B_j^2-\lambda_j^2)\right]\ . \tag{24}$$

The nonzero Lyapunov exponents are calculated as $\pm\langle\rho\rangle$.

VII. RESULTS

We now consider a specific example. The case where only the center element is initially excited is chosen to define the fiducial trajectory. A perturbation vector is selected to track the growth of small perturbations using the mapping given in Eqs. (21)–(23). The perturbation vector can be chosen quite arbitrarily for the purposes of characterizing the steady-state behavior. However, the initial vector direction set by the phase angle α does determine the length of the transient which occurs in the antisymmetric subspace before exponential growth locks the perturbation. Here, the initial phase angle α of the perturbation vector is chosen to be the finite precision arithmetic approximation to $-\pi/4$. The vector with phase angle $-\pi/4$ is one of the rare vectors pointing in the direction of contraction in the limit $Q\to 0$ [10]. The local exponent seen by the tracking vector is plotted as a function of z for three values of Q in Fig. 3. The bounding ellipse limits are also shown in the figure. The transient occurring before locking by the fiducial trajectory is evident, caused by initial mismatching of the vector direction with the direction of largest growth. At $Q=0.4$ this transient is long lived owing to its proximity to the direction of contraction. Indeed, the local exponent follows the lower bounding ellipse limit for several cycles. The initial direction of contraction has rotated at higher values of Q so that the transient is shorter lived.

The exponents vary periodically in the steady state, with period determined by the fiducial trajectory. At low Q values, the local exponent perfectly matches the upper bounding ellipse limit throughout the period of the motion. Chaos is present, since the average value of the exponent is positive. As a result of the match between the orientation of the perturbation vector and the major axis, the asymptotic value of ρ in the low-Q limit can

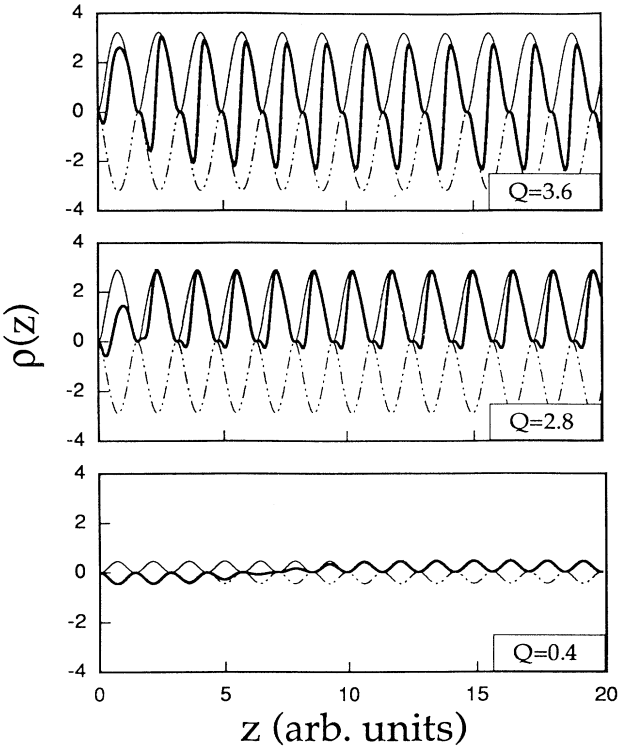

FIG. 3. Periodic variation of the local exponent as detected by an arbitrary linearized tracking vector for three values of Q. The bounding ellipse limits are also shown. Thick solid line, local exponent $\rho(z)$. Thin solid line, upper limit set by bounding ellipse. Dashed line, lower limit set by bounding ellipse.

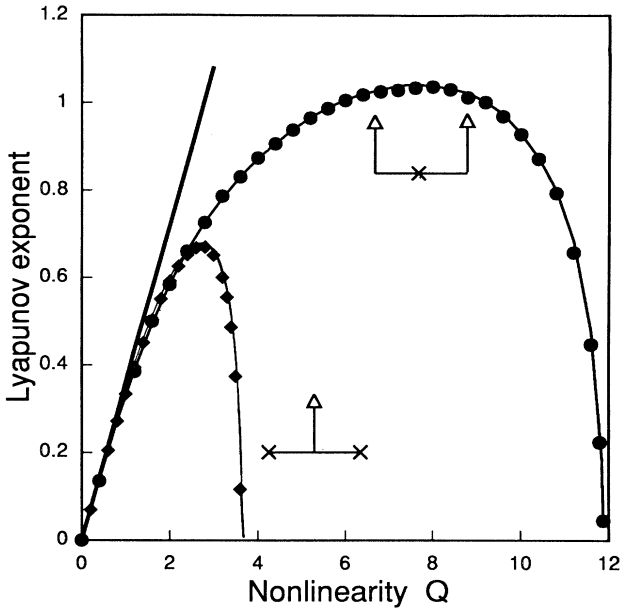

FIG. 4. Lyapunov exponent as a function of nonlinear parameter Q, for two different fiducial trajectories. The single arrow schematic represents a fiducial trajectory in which the field is initially launched into the center lattice element. The schematic with two arrows represents a fiducial trajectory where the two outer elements are equally excited. Thin line, numerical calculation. Filled symbols, calculation based on motion of small perturbations localized in the antisymmetric subspace. Thick solid line, asymptotic result.

then be derived directly from the average value of Eq. (20), given by

$$\langle \rho \rangle \underset{Q \to 0}{\sim} \frac{Q}{4 \ln 2} . \tag{25}$$

This result is in agreement with previous calculations [4,10] and is clearly a consequence of the length scaling properties of the resonant Hamiltonian as discussed in Sec. II.

At higher Q, the tracking vector starts to precess around the ellipse major axis. Such new effects are unsurprising since it is a standard feature of Hamiltonian nonlinear dynamics that various terms in the system Hamiltonian can be brought in and out of resonance by the influence of nonlinearity [1]. At higher Q therefore the tracking vector does not follow the upper bounding ellipse limit over the full period. Indeed, local contraction of the tracking vector occurs which causes the lower ellipse limit to be approached. At the critical value $Q \approx 3.6$ the tracking vector experiences expansion and contraction equally and there is a transition from chaotic to regular motion. This high-nonlinearity transition can be interpreted in terms of the usual KAM theory where the movement of resonances due to nonlinearity leads to stabilization of the motion.

The dependence of the positive Lyapunov exponent on Q is plotted in Fig. 4, for two different fiducial trajectories. In one case, the center oscillator is excited initially, whereas in the other case the two outer oscillators are excited initially. Values calculated using the method previously described [4] are also shown. Excellent agreement is obtained between the procedure described here and the previous numerical results. In addition, the asymptotic result is shown to predict the low Q limiting behavior correctly, in line with the behavior expected for a resonant Hamiltonian. The Lyapunov exponent is always positive for any sufficiently small yet nonzero field, confirming the presence of microchaos in this system. For the center-excite condition, all Lyapunov exponents become zero at $Q \sim 3.6$ and remain so at all higher values of Q. For the outer-excite condition, this "stochastic-regular" transition occurs at $Q \sim 12$.

VIII. CONCLUSIONS

To summarize, we have investigated particular characteristic of chaos in a three-element DNLSE lattice. By partitioning the phase space into symmetric and antisymmetric subspaces and taking advantage of the integrability of the symmetric excitations, we have been able to demonstrate that the motion of a two-dimensional vector in the antisymmetric subspace is sufficient to characterize chaotic motion in the vicinity of symmetric excitations, i.e., the chaos is localized. Furthermore, we have

confirmed that the three-element DNLSE exhibits the instability we call "microchaos," i.e., chaos at arbitrarily low nonlinearity. Both microchaoticity and localization occur as a result of certain symmetries in the motion and it would be useful to examine more general connections linking these two features. In conclusion, we agree with the pioneers in this field [2] that the microchaotic instability is likely to be a universal phenomenon and one that manifestly deserves further investigation.

ACKNOWLEDGMENTS

The work reported here was partially supported by the ESPRIT Basic Research Contract No. 7118 (TONICS) of the Commission of the European Communities. One of the authors (L.J.B.) wishes to acknowledge support from the University of California and the U.S. Department of Energy (under Contract No. DE-FG03-86ER13606-A003).

[1] A. J. Lichtenberg and M. A. Lieberman, *Regular and Stochastic Motion* (Springer-Verlag, New York, 1983).
[2] J. Ford and G. H. Lunsford, Phys. Rev. A **1**, 59 (1970).
[3] G. Contopolous, Cel. Mech. **17**, 167 (1978).
[4] K. W. DeLong, J. Yumoto, and N. Finlayson, Physica D **54**, 36 (1991).
[5] V. M. Kenkre and D. K. Campbell, Phys. Rev. B **34**, 4959 (1986). The DNLSE is a special case of a more general system of equations known as the discrete self-trapping equation (DSTE) [J. C. Eilbeck, P. S. Lomdahl, and A. C. Scott, Physica D **16**, 318 (1985)].
[6] D. N. Christodoulides and R. I. Joseph, Opt. Lett. **13**, 794 (1988).
[7] N. Finlayson and G. I. Stegeman, Appl. Phys. Lett. **56**, 2276 (1990).
[8] Y. Chen, A. W. Snyder, and D. J. Mitchell, Electron. Lett. **26**, 77 (1990).
[9] C. Schmidt-Hattenberger, R. Muschall, U. Trutschel, and F. Lederer, Opt. Quantum Electron. **24**, 691 (1992).
[10] L. J. Bernstein, Opt. Commun. **96**, 406 (1992).
[11] A. Wolf, J. B. Swift, H. L. Swinney, and J. A. Vastano, Physica D **16**, 285 (1985).
[12] E. T. Whittaker and G. N. Watson, *A Course of Modern Analysis* (Cambridge University Press, Cambridge, England, 1963).